TICT Formation in Para- and Meta-Derivatives of *N*-Phenylpyrrole

Sukumaran Murali and Wolfgang Rettig*

Humboldt University of Berlin, Brook-Taylor-Strasse 2, D-12489 Berlin, Germany

Received: July 14, 2005; In Final Form: November 1, 2005

The photophysical properties of *m*- and *p*-cyano *N*-phenylpyrrole (*m*- and *p*-PBN) are compared. Both compounds show highly red-shifted and strongly forbidden emission in polar solvents, assigned to a charge transfer state. The forbidden nature is indicative of very weak coupling between the two π-systems, and a twisted emissive structure is suggested (TICT state). Comparison to quantum chemical calculations indicates that the twisted structure possesses an antiquinoid distortion of the benzonitrile group, i.e., the central bonds in the ring are lengthened instead of shortened. *m*-PBN is the first meta compound which shows a CT emission assignable to a TICT state. It differs from *p*-PBN by a less exergonic formation of the CT state from the LE/ICT quinoid state. Consequently, it shows only single LE/ICT fluorescence in nonpolar alkane solvents, whereas *p*-PBN shows dual fluorescence in this solvent (LE/ICT and TICT).

1. Introduction

Since the ''twisted intramolecular charge transfer" (TICT) concept[1] had been developed some 2 decades ago, the investigation of charge transfer (CT) in donor−acceptor systems, especially substituted benzenes, has led to the understanding of the dual fluorescence of 4-cyano-*N*,*N*-dimethylaniline (DMABN) which was discovered by Lippert in 1959.[2] TICT states are formed via an adiabatic photoreaction: If a TICT forming molecule possessing a planar ground state is electronically excited, it relaxes spontaneously in the excited state toward a twisted conformation from where it decays by redshifted emission or nonradiatively. The rate of reaching the TICT state with its twisted conformation is determined, at least for compounds similar to DMABN and apart from other factors, by the initial (Franck−Condon) twist angle which is reached directly after light absorption from the ground state. The closer this initial twist angle is to the final one (about 90°), the faster is the TICT population kinetics. In that respect, CT can be explored by variation of the donor and acceptor groups on either side of the benzene moiety stabilizing the CT transfer state. Surprisingly, the dual fluorescence has not been observed in the case of meta derivatives of DMABN.[3,4] This is in part due to the larger energy gap between the first two excited states (^1L_a, ^1L_b) for the meta as compared to the para derivatives, and therefore the driving force for the adiabatic photoreaction is reduced for *m*-DMABN as compared to *p*-DMABN.[1]

Pyrrolobenzonitriles constitute a group of donor−acceptor systems in which the dimethylamino group is replaced by a better donor moiety, namely pyrrole. The absorption and fluorescence properties of *N*-pyrrolobenzonitrile (*p*-PBN), its ester derivative PBAEE, and a more twisted model compound DPBN with stronger donor−acceptor properties have been compared by Gude et al.[5] Recently, Yoshihara et al.[6] reported on the determination of excited-state dipole moments of *N*-phenylpyrroles and DMABN from solvatochromic and thermochromic measurements. Both the para and meta PBN derivatives were shown to populate a CT excited state but the conformational nature remained unclear because transition moments were not determined.

Zilberg et al.[7] performed theoretical calculations on *N*-phenylpyrroles. The calculations support the possible existence of two distinct structures for the CT state. One of them has a quinoid geometry with characteristically shortened central bonds in the benzene ring, and the benzene and pyrrole rings are coplanar at the energy minimum. The other state is of antiquinoid geometry (where the central benzene bonds are lengthened instead of shortened), has a larger dipole moment than the quinoid one, and has an energy minimum with the pyrrolo group twisted by 90° with respect to the benzene ring.

The perpendicular antiquinoid state is expected to possess forbidden emissive properties while the quinoid state is of an allowed nature. Our results reveal that the CT emission is strongly forbidden in both compounds investigated. The combination of experiment and theory therefore leads to the conclusion of antiquinoid properties and twisted structure of the emitting CT state in both compounds.

The meta isomer of *p*-PBN, *m*-PBN is the first compound where a meta-substituted cyano derivative shows TICT formation. Like *m*-DMABN, *m*-PBN also shows a red-shift in the absorption maximum of S_1. This reduces the exothermicity of CT formation for meta-compounds in general. On the other hand, when comparing *p*-PBN with DMABN, there is a larger exothermicity for the LE to TICT formation due to the better pyrrole donor. As a matter of fact, already nonpolar solvents like *n*-hexane induce the appearance of dual fluorescence for *p*-PBN but not for DMABN.

2. Experimental Section

2.1. Materials. The compounds were synthesized according to the procedures described in refs 8 and 9 and sublimed. The purity has been checked by thin-layer chromatography (TLC). All solvents used for the spectroscopic measurements were of spectrophotometric grade (Merck Uvasol).

2.2. Steady-State Spectra. Absorption spectra were measured on an ATI UNICAM UV Series spectrometer UV4−21113. All steady-state fluorescence spectra were measured by using an SLM Aminco-Bowman series 2 spectrofluorimeter fitted with

* Corresponding author.

10.1021/jp053878r CCC: $33.50
Published on Web 12/10/2005

a 150 W xenon lamp and a 2 nm excitation and emission bandpass. All fluorescence spectra were corrected for detector response.

2.3. Fluorescence Quantum Yields. The quantum yields of fluorescence were measured relative to quinine bisulfate in 0.1 N H_2SO_4 and calculated on the basis of eq 1[10]

$$\phi_f = \phi_f^0 \frac{n^2}{n_0^2} \frac{A^0}{A} \frac{\int I_f(\lambda_f)\, d\lambda_f}{\int I_f^0(\lambda_f)\, d\lambda_f} \quad (1)$$

where n_0 and n are the refractive indices of the solvent, A^0 and A (≤ 0.1) are the absorbances, $\phi_f{}^0$ (= 52%)[11] and ϕ_f are the quantum yields, and the integrals denote the (computed) area of the corrected fluorescence bands, each parameter being for the standard (index 0) and the sample solution, respectively. The relative experimental error of the quantum yields is around ±10%.

2.4. Fluorescence Lifetime. The fluorescence decay measurements were performed using time correlated single photon counting (TCSPC).[12] Synchrotron radiation from the Berlin Synchrotron facility BESSY II was used as light source in conjunction with an excitation monochromator (Jobin Yvon, II, 10 UV). It delivers a 1.25 MHz pulse train with characteristic pulse widths of 30−50 ps. The fluorescence and decays were detected by a microchannel plate photomultiplier (MCP, Hamamatsu R 1564-U-01) cooled to −30 °C, coupled to an emission monochromator (Jobin Yvon II, 10 VIR) by means of quartz fiber optics. The signal from a constant fraction discriminator (CFD, Tennelec 454) was used as the start pulse for the time-to-amplitude converter (TAC, Tennelec TC864) operating in the reverse mode. The BESSY II synchronization pulse was used as the stop pulse. The MCP pulses were amplified by an amplifier (INA 10386) and coupled into the CFD. A multichannel analyzer (Fast Comtec MCDLAP) was used for data accumulation. The decays were analyzed by the "least squares" and iterative reconvolution method on the basis of the Marquardt−Levenberg algorithm, which is implemented in the commercial global analysis program.[13] The instrument response function was obtained by the detection of Rayleigh scattered light in a scattering solution and had a width of 120 ps. The quality of the exponential fits was evaluated on the basis of the reduced χ^2 values.

2.5. Quantum Chemical Calculations. The semiempirical calculations reported in the present work included full geometry optimization in the ground state without configuration interaction using the AM1 method[14] contained in the AMPAC program package.[15] Single point calculations for the Franck−Condon excited states were performed by taking the fixed optimized ground-state geometry and using configuration interaction including 300−400 singly and multiply excited configurations constructed on the basis of the central 16 molecular orbitals.

The ab initio calculations were performed with GAMESS[16] using the cc-pVDZ basis set.[17] Full geometry optimization was performed for the doublet ground state of benzonitrile radical anion by using CASSCF calculations (CAS(11/10)/cc-pVDZ (11 electrons on 10 orbitals)).

3. Results

3.1. Room-Temperature Spectroscopy. The absorption and emission spectra of *p*-PBN and *m*-PBN in various solvents of different polarity are compared in Figure 1. The main absorption band of *m*-PBN is shifted to the blue region compared to *p*-PBN in *n*-hexane. There is also a weak shoulder in the red edge of

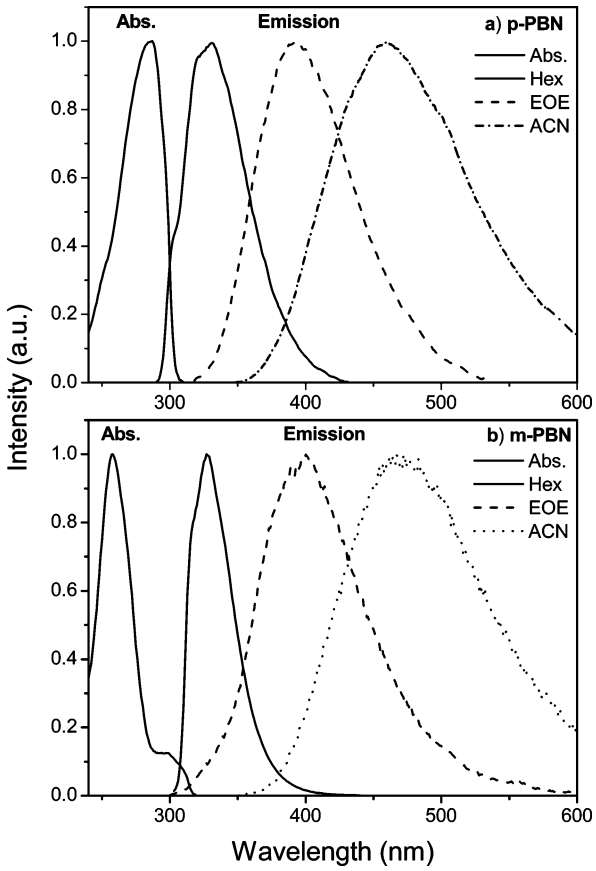

Figure 1. Normalized absorption and fluorescence spectra of *p*-PBN and *m*-PBN in various solvents of different polarity (Hex, *n*-hexane; EOE, diethyl ether; ACN, acetonitrile).

the absorption spectrum of *m*-PBN, which can be interpreted as a weak transition, which is red-shifted when compared to the corresponding one in *p*-PBN. All the emission spectra exhibit a strong red-shift of their maxima increasing from weakly polar to strongly polar solvents. The emission of *p*-PBN in *n*-hexane is broad as compared to the narrower band in *m*-PBN. Yoshihara et al.[6] reported dual fluorescence for *m*-PBN dissolved in the medium polar solvent diethyl ether (EOE). This is has been verified here by comparing an aerated and a deaerated solution, and the shoulder in the fluorescence spectrum is not present for both freshly prepared solutions but rises for the aerated solution only for a prolonged stay of the sample in the dark. The shoulder reported in ref 6 is therefore assigned to the appearance of a thermal oxidation product. No shoulder appeared on photolysis of the deaerated solution. Emission maxima observed in this work differ somewhat from the previous work of Gude et al.[5] and Yoshihara et al.[6] due to the use of different fluorescence spectrometers and correction curves. The quality of the emission correction curve is especially important for broad and structureless CT spectra as observed for *m*-PBN and *p*-PBN in polar solvents. We have verified the quality of the correction curve used here by comparing to spectra measured on a freshly calibrated fluorimeter.

Comparison of the spectra of *m*-PBN with *p*-PBN exhibits rather similar features except in nonpolar solvents such as *n*-hexane where the emission spectrum is narrower for *m*-PBN than for *p*-PBN in *n*-hexane. The solvatochromic red-shift in going from low to high polar solvents is a substantial indication of the charge transfer (CT) nature of the emitting state in both compounds. (see section 3.2)

The molar extinction coefficient values determined for *p*-PBN and *m*-PBN in *n*-hexane are $\epsilon\ (\lambda_{287}^{max})$ = 25 747 and $\epsilon\ (\lambda_{258}^{max})$

TABLE 1: Photophysical Characteristics of *m*-PBN and *p*-PBN in Solvents of Different Polarity at Room Temperature

	sol	λ_{flu} (nm)	$\Delta\nu_{st}$[c] (cm^{-1})	ϕ_f	τ_f (ns)	k_f (10^7 s^{-1})	k_{nr} (10^8 s^{-1})	M_f (D)
***m*-PBN**[a,b]	Hex	327	2752	0.155	3.31	4.68	2.5	4.47
	BOB	369	6233	0.023	-			
	EOE	397	8144	0.019	3.76	0.47	2.6	1.94
	THF	429	10 023	0.016	5.01	0.32	1.9	1.70
	DCM	415	9236	0.013				
	ACN	476	12 324	0.013	5.35	0.24	1.8	1.85
***p*-PBN**[d]	Hex	332	4722	0.077	2.42[e]	3.18	3.8	3.77
	EOE	393	9397	0.023	3.80[e]	0.61	2.6	2.18
	THF	422	11 146	0.024				-
	DCM	412	10 571	0.022	3.10[e]	0.71	3.2	2.35
	ACN	460	13 104	0.024	8.20[e]	0.29	1.2	1.93

[a] $\lambda_{max} = 258$ nm used as excitation wavelength for all solvents. [b] S_1 corresponds to the shoulder at 300 nm in the absorption spectrum. [c] The Stokes shift is measured from the weak absorption shoulder at 300 nm. [d] $\lambda_{max}^{exc} = 287$ nm. [e] From ref 5.

$= 25\,400$, respectively. In the case of *p*-PBN, the bands due to the S_1 and S_2 states are strongly overlapping (see below), whereas the redshift of the S_1 absorption in *m*-PBN leads to the appearance of the shoulder with small extinction coefficient in the absorption spectrum (Figure 1). The blue shift of the main absorption band (see Figure 1) and the small absorption shoulder at ca. 300 nm for *m*-PBN is a consequence of the meta-effect.[18] As the calculations described below show, the single main absorption band of *p*-PBN hides a weak band, which can be assigned to the ^1L_b state in Platt's nomenclature. Because of the meta-effect, the S_1 state of *m*-PBN is therefore at lower energy than for *p*-PBN.

Stokes shift values with reference to the first absorption band have been calculated and are tabulated for both *m*-PBN and *p*-PBN in Table 1. It is found that they are slightly smaller for *m*-PBN due to the red-shift of S_1. But in the case of highly polar solvents, the Stokes shift increases very strongly for both compounds indicating emission from a CT state. The fluorescence decay curves are monoexponential, allowing the evaluation of radiative and nonradiative rate constants according to eqs 2 and 3. In eq 3, k_{nrn}^{tot} corresponds to the sum of all nonradiative processes including triplet formation. The emission transition dipole moments were calculated using eq 4[19] and are the characteristics of the excited states. The measured data and calculated photophysical values are collected in Table 1.

$$k_f = \phi_f/\tau_f \tag{2}$$

$$k_{nrn}^{tot} = k_f(\phi_f^{-1} - 1) \tag{3}$$

$$M_f^2 = (3hk_f/64\pi^4 n^3 \nu_f^3) \tag{4}$$

The k_f values decrease when going from hexane to polar solvents in parallel to the quantum yield values for both *p*-PBN and *m*-PBN. In the case of *m*-PBN, the k_f values in the more polar solvents are even smaller than in *p*-PBN, indicating the enhancement of forbidden character present in the emitting state.

3.2. Solvatochromic Measurements. The solvatochromic slopes were analyzed to get quantitative information on the dipole moments for both compounds, by applying the Mataga equation (eq 5),[20] and the resulting values are collected in Table 2. The plot of the emission maximum vs the polarity parameter $\Delta f'$ is shown in Figure 2. Similarly, an alternative type of Mataga plot has also been made by using low-temperature fluorescence spectra: In this case, the emission maxima at different temperatures in diethyl ether were plotted vs the temperature dependent $\Delta f'$ values (Figure 3.) In this case, $\Delta f'$ was calculated by taking dielectric constant, ϵ and refractive index, *n* as a function of temperature.[21] The plots show a linear relationship in both cases. It is found that the solvatochromic

TABLE 2: Results of the Solvatochromic Measurements at Room Temperature and Low Temperature (Solvatochromic Slopes, Assumed Onsager Factor *a*, μ_g (D) and Derived μ_e (D) Using Two Different Methods)

	a (Å)[a]	slope (10^3 cm^{-1})[b]	slope (10^3 cm^{-1})[c]	μ_g (D)[d]	μ_e (D)
p-PBN	4.1	−27.5[e]	−27.5	2.09	14.8
	4.1	−35.5[f]		2.09	16.6
m-PBN	4.1	−30.4[e]	−28.0	2.78	15.8
	4.1	−40.1[f]		2.78	18.0

[a] Calculated from mass−density formula. [b] Error less than 10%. [c] From ref 5. [d] Calculated by AM1. [e] From the Mataga plot at room temperature. [f] From the Mataga plot in diethyl ether at low temperatures.

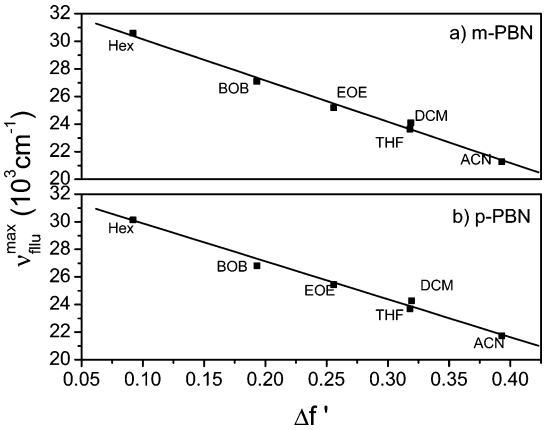

Figure 2. Solvatochromic fluorescence plot of (a) *m*-PBN and (b) *p*-PBN derived from differently polar solvents at room temperature (Hex, *n*-hexane; BOB, dibutyl ether; EOE, diethyl ether; THF, tetrahydrofuran; DCM, dichloromethane; ACN, acetonitrile).

slope values (Table 2), which are determined from the second type of Mataga plot at different temperatures, are somewhat larger than from the room-temperature Mataga plot, but in both types of Mataga plots, the slope values are slightly higher for *m*-PBN than for *p*-PBN. The Onsager radius, a = 4.1 Å for *p*-PBN[5] and *m*-PBN was calculated by the mass−density formula (eq 6)[22] by taking an average density $\rho = 0.95$ g/cm.[5] This approach neglects the different molecular shapes of *p*-PBN and *m*-PBN.

$$\nu_f = -\frac{2\Delta f'}{4\pi\epsilon_0 hca^3}\mu_e(\mu_e - \mu_g) + \text{const} \tag{5}$$

where $\Delta f' = (\epsilon - 1)/(2\epsilon + 1) - {}^1/_2(n^2 - 1)/(2n^2 + 1)$

$$a = \sqrt[3]{3M/4\pi N_A \rho} \tag{6}$$

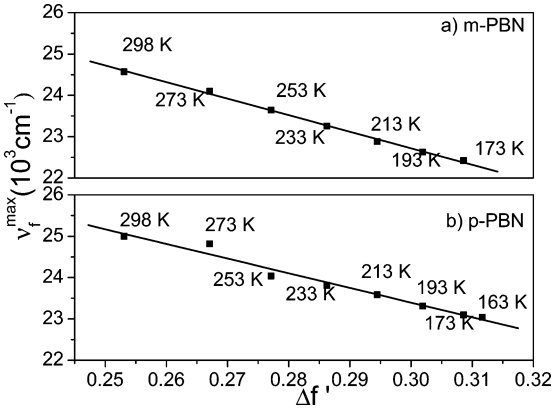

Figure 3. Solvatochromic fluorescence plot of (a) *m*-PBN and (b) *p*-PBN derived from measurements in diethyl ether at variable temperature.

In the above equations, μ_e and μ_g are the excited and ground-state dipole moments respectively, h is Planck's constant, c is the velocity of light, and n and ϵ are the refractive index and dielectric constant, respectively. The resulting excited state dipole moments are determined using the calculated ground state dipole moments and are very close for both solvatochromic methods and are even slightly larger for *m*-PBN as compared to *p*-PBN (Table 2). These large μ_e values suggest that the emissive state is of CT nature and is similar in both compounds regardless of the position of the cyano substituent.

3.3. Spectroscopic Measurements at Low Temperatures. Fluorescence measurements at low temperatures were done in the nonpolar solvent mixture methylcyclohexane−isopentane (1:4) and in the medium polar solvent diethyl ether. For *m*-PBN in EOE, with the lowering of temperature, a red-shift of the emission maxima is observed (Figure 3) and analyzed using the Mataga equation. A red-shift of the emission has also been observed for *p*-PBN in EOE. This thermochromic red-shift is mainly due to the enhancement of the dielectric constant and the refractive index with the lowering of temperature and can be ascribed to the stabilization of the CT state.

Neither for *p*-PBN nor for *m*-PBN does the low-temperature spectra in EOE (Figure 4) show an indication of dual fluorescence. However, a more complex spectral behavior is exhibited by the development of the vibrational structure for *p*-PBN and *m*-PBN in the nonpolar solvent mixture (MCH-IP), upon cooling (Figure 5).

Upon cooling, the behavior of *m*-PBN and *p*-PBN in the alkane solvent is opposite: Whereas the highest energy vibronic band is enhanced in *m*-PBN upon cooling, this spectral feature diminishes for *p*-PBN at low temperature. Moreover, the spectra are significantly broader for *p*-PBN. The behavior of *m*-PBN can be understood as the normal behavior at low temperature, where the structuring of vibronic bands is enhanced upon cooling. The diminishing of the vibronic feature at around 305 nm for *p*-PBN at low temperature can then be understood as the result of dual fluorescence, with an LE/CT excited state equilibrium and a thermodynamically more stable CT state.[5]

Upon closer inspection, the 0−0 vibronic band is seen to be situated at lower energy in *m*-PBN (∼316 nm) than in *p*-PBN (∼305 nm) reflecting the decreased energy of the emitting LE state for *m*-PBN (meta-effect), as is already visible in the absorption spectrum (see section 3.1 above).

3.4. Computational Results. 3.4.1. AM1 Calculations. The ground-state optimized geometries of the benzonitrile radical anion, *p*-PBN and *m*-PBN as calculated by using the AM1 method are shown in Figure 6. Table 3 shows the equilibrium

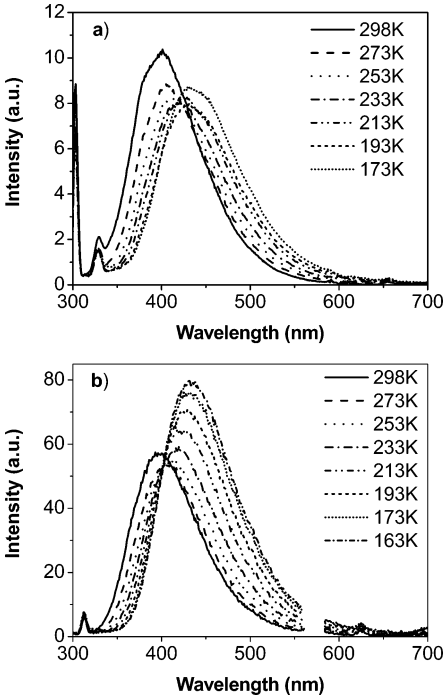

Figure 4. Low-temperature fluorescence spectra of (a) *m*-PBN and (b) *p*-PBN in diethyl ether (EOE). For part b, the second-order Rayleigh scattering in the spectral region 560−585 nm has been omitted.

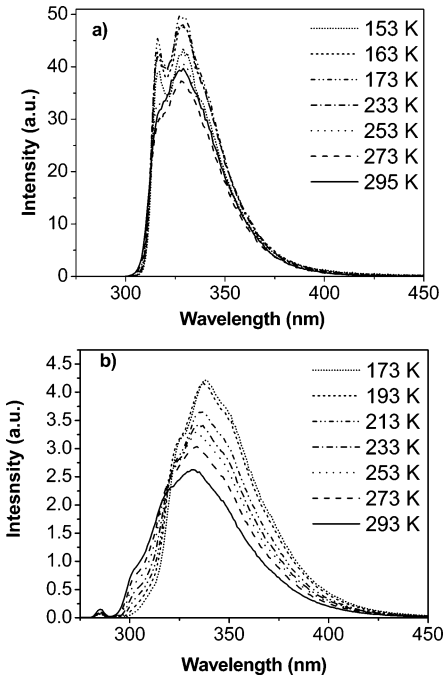

Figure 5. Low-temperature fluorescence spectra of (a) *m*-PBN and (b) *p*-PBN in the nonpolar solvent mixture methylcyclohexane: isopentane, MCH/IP (1:4).

twist angles, rotational barriers to planarity and perpendicularity as well as dipole moments, which were calculated for the ground state. These values are compared with the parent compound, *N*-phenylpyrrole (PB). The twist angle and rotational barrier for *m*-PBN are slightly higher than for *p*-PBN, but comparable with PB. The rotational barrier for *m*-PBN and PB to reach the perpendicular geometry is less than for *p*-PBN due to their more twisted nature in the equilibrium geometry and smaller inter-moiety mesomeric contribution.

The three ground-state optimized conformations (equilibrium twist angle, as well as planar and perpendicular one) were also

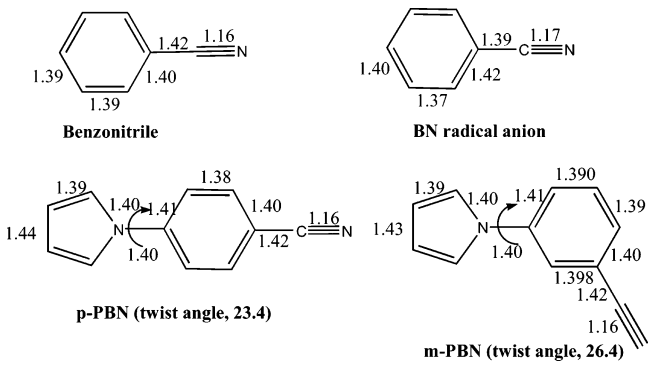

Figure 6. Equilibrium structures of benzonitrile (BN), BN radical anion, *p*-PBN, and *m*-PBN in the S_0 state.

TABLE 3: Equilibrium Twist Angles, Rotational Barriers to Each the Planar and the Perpendicular Geometry and Dipole Moments in the S_0 State as Calculated by AM1

molecules	eq twist angle (deg)	ΔE_{planar} (kcal/mol)	ΔE_{perp} (kcal/mol)	μ_0 (D)
p-PBN	23.3	0.27	2.59	2.09
m-PBN	26.4	0.40	2.05	2.78
PB	26.5	0.39	2.01	1.77

analyzed regarding excited-state energies and properties. Configuration interaction (CI) for the excited states was used. The calculated values of transition energy, relative energy, dipole moments and oscillator strengths of the low lying excited states are collected in Table 4 and are discussed below.

3.4.2. CASSCF Calculations. The results on *p*-PBN have been given in detail previously.[7] The most important observation was that the charge-transfer excited state of A symmetry has two minima on the hypersurface which involve both changes in the twist angle α between the pyrrole and the benzene ring as well as characteristic bond length changes in the benzene ring. The so-called quinoid minimum is situated at $\alpha = 0°$ (planarity), and the central bonds in the benzene ring are shortened, characteristic for a quinoid distortion. On the other hand, the so-called antiquinoid minimum AQ is characterized by a perpendicular structure ($\alpha = 90°$) and by long central benzene bonds, which are longer than the adjacent ones.

In the AQ minimum at perpendicularity, the orbitals involved in the charge transfer state of symmetry A (HOMO-1 P_b to LUMO B_b; see Table 4 and Figure 7), are localized on the subunits (Figure 7 shows the near-planar equilibrium conformation where HOMO-1 is delocalized (P_bB_b) but this delocalization vanishes at 90° twist), so that the dipole moment is very high (16 D from the AM1 calculations reported in Table 4; the dipole moment value from the CASSCF calculations is 16.2 whereas for the quinoid minimum Q at planarity, the HOMO-1 is strongly delocalized over both rings (see Figure 7: P_bB_b), and the calculated dipole moment is smaller (4.9 D from AM1 and 11.0 D from CASSCF). Note that according to the AM1 calculations (without geometry optimization in the excited state), the energy of the AQ state is very high (S_7), so that the Q state is the lowest CT state (S_2). The CASSCF calculations with geometry optimization in the excited state lower especially the AQ state, so that its minimum becomes lower lying than the minimum of the quinoid state Q, with an energy difference of 0.55 eV in the gas phase.

The calculations in Table 4, and also the results of Parusel[33] indicate that with semiempirical calculations for the 90° twisted geometry in the ground state (with optimized bond lengths), AQ is not the lowest CT state but a state B (90°) of B symmetry (S_3, involving HOMO and LUMO orbitals P_a and B_b. The dipole moments are very large in both perpendicular (18 D) and planar conformation (^{1}B(0°) state with 11.7 D) because the orbitals are rather localized even for the planar geometry. Of course, geometry relaxation is again expected to lead to changes in the relative ordering of ^{1}B(0°) and ^{1}B(90°). The energetics of this B−CT state has not yet been calculated with CASSCF geometry optimization. But the arguments and results given below indicate, that the same Q and AQ isomers should also be expected for this state of different symmetry from the Q and AQ state reported by Zilberg et al.[7]

Because of the decoupled orbitals in the perpendicular conformation, the CT state can be regarded as the combination of an anion radical of benzonitrile and a cation radical of pyrrole. We can therefore expect to get a deeper insight by a closer look on the benzonitrile anion radical alone, which is of doublet electronic structure but can be calculated as open-shell ground state molecule with somewhat simpler geometry optimization than for the excited state of PBN, and it can readily be treated with the CASSCF calculations.

The electronic structure of the benzonitrile anion radical is determined by the occupancy of the doubly occupied and one singly occupied orbital. In addition to the two relevant occupied orbitals, benzonitrile has three low-lying unoccupied MO's, which provide its acceptor ability:

The first two MOs in Figure 8 are normal π orbitals perpendicular to the benzene plane, corresponding to B_b^L and B_a^L in Figure 7. If the lone electron occupies the b_1 MO, this leads to a 1^2B_1 electronic state of the anion-radical where the lone electron is delocalized on both benzene ring and cyano group. If the lone electron occupies the a_2 orbital, the 1^2A_2 electronic state of the anion radical is formed, without participation of the cyano substituent. Occupation of MO b_1 with one electron leads to a 1^2B_1 electronic state with no participation of the cyano substituent. Occupation of the b_2 orbitals leads to localization of the lone electron on the cyano group.

The choice of the active space for the CASSCF calculations was dictated by the need to take into account all three possible situations. The active space therefore includes four occupied π_x and four unoccupied π_x* orbitals, as well as the orthogonal π_y-system of the CN group: one occupied π_y and one unoccupied π_y*. The results of the CAS(11/10)/cc-pVDZ calculations (11electrons on 10 orbitals) show the following results:

(a) The optimized 1^2B_1 state has a quinoidal structure (see Figure 9 for the bond lengths, with the atomic charges given in square brackets (Löwdin atomic populations) distributed between the benzene ring and the CN group.

(b) The 1^2A_2 state has an anti-quinoidal structure with the lone electron delocalized on the benzene ring only and possessing lengthened central benzene bonds.

(c) The 1^2B_2 state has a lengthened CN bond with the charge localized on the CN group.

The 1^2A_2 electronic state crosses the 1^2B_1 state along the relaxation coordinate connecting these two states, but it is situated 13.3 kcal/mol above the global minimum. The 1^2B_2 state is an excited state of the anion radical and 67.4 kcal/mol above the global minimum.

4. Discussion

4.1. Absorption. Excited states of donor−acceptor para-substituted benzenes possess two close lying π,π* excited states: the long axis polarized ^1L_a-type constituting the main long wavelength absorption band and a perpendicularly polarized ^1L_b-type state with much weaker absorption intensity. In the gas phase, these bands are discernible for *p*-PBN;[23] in solution,

TABLE 4: Results of Semiempirical AM1-CI Calculations for *p*-PBN and *m*-PBN in the Planar, the Equilibrium, and the Perpendicular Ground State Geometry with Optimized Bond Lengths

compounds	geometry	state	excitation energy (eV)	dipole moment (D)	oscillator strength (*f*)	CI analysis[a,b]	orbital nature and symmetry of the CT states[c]
p-PBN	planar (0°)	S_0		2.18			
		S_1	3.89	4.03	0.0002	31−33 (48%)	$B_a \rightarrow B_b(B)$, **^1L_b**
						29−32 (36%)	
		S_2	3.94	5.23	0.4222	31−32 (76%)	$P_bB_b \rightarrow B_b(A)$, **$^1L_a$**
		S_3	4.45	10.76	0.0237	30−32 (74%)	$P_a \rightarrow B_b(B)$, **CT1(B)**
		S_4	4.64	6.88	0.0000	30−35 (90%)	
		S_5	4.83	2.79	0.0195	30−37 (32%)	
						31−34 (30%)	
p-PBN	eq (23.3°)	S_0		2.08			
		S_1	3.99	3.92	0.0000	29−32 (38%)	$B_a \rightarrow B_b(B)$
						30−33 (46%)	$P_bB_b \rightarrow B_a(B)$
		S_2	4.02	4.78	0.3525	30−32 (68%)	$P_bB_b \rightarrow B_b(A)$
		S_3	4.47	11.65	0.0239	31−32 (76%)	$P_a \rightarrow B_b(B)$, **CT1(B)**
		S_4	4.73	7.13	0.0053	31−35 (80%)	
		S_5	4.74	3.78	0.0561	31−38 (28%)	
						31−35 (12%)	
p-PBN	(90°)	S_0		1.11			
		S_1	4.17	1.21	0.0030	28−32 (48%)	$B_a \rightarrow B_b(B)$
						29−33 (44%)	$B_b \rightarrow B_a(B)$
		S_2	4.47	0.83	0.0108	30−34 (36%)	$P_b \rightarrow P_b(A)$
						31−38 (44%)	$P_a \rightarrow P_a(A)$
		S_3	4.79	17.97	0.0009	31−32 (88%)	**CT1(B)**, $P_a \rightarrow B_b$
		S_4	4.81	7.04	0.0000	31−37 (92%)	
		S_5	4.91	1.39	0.1565	29−32 (66%)	
						28−33 (30%)	
		S_6	5.12	0.72	0.0705	31−34 (78%)	
		S_7	5.14	16.02	0.0000	30−32 (86%)	**CT2(A)**, $P_b \rightarrow B_b$
		S_8	5.26	6.32	0.0223	30−32 (86%)	
		S_9	5.46	17.21	0.0025	31−33 (90%)	**CT3(A)**, $P_a \rightarrow B_a$
		S_{10}	5.93	15.02	0.0011	30−33 (84%)	**CT4(B)**, $P_b \rightarrow B_a$
m-PBN[d]	planar (0°) fix	S_0		2.85			
		S_1	3.72	4.03	0.0123	31−32 (30%)	$P_bB_b \rightarrow B_b(A)$
						31−33 (22%)	$P_bB_b \rightarrow B_b(A)$
		S_2	4.08	3.70	0.2562	31−32 (32%)	$P_bB_b \rightarrow B_b(A)$
						31−33 (38%)	$P_bB_b \rightarrow B_b(A)$
		S_3	4.53	7.21	0.0269	30−33 (34%)	$P_a \rightarrow B_b(B)$
						30−32 (38%)	$P_a \rightarrow B_b(B)$, **CT1**
		S_4	4.79	3.15	0.0230	30−38 (22%)	
						31−34 (26%)	
		S_5	4.98	7.38	0.0000	30−35 (54%)	
						30−36 (40%)	
m-PBN[d]	eq.(26.4°)	S_0		2.75			
		S_1	3.80	3.67	0.0073	30−32 (28%)	$P_bB_b \rightarrow B_b(A)$
						29−32 (14%)	$B_a \rightarrow B_b(B)$
		S_2	4.15	3.64	0.2233	30−33 (38%)	$P_bB_b \rightarrow B_b(A)$
						30−32 (28%)	$P_bB_b \rightarrow B_b(A)$
		S_3	4.59	7.47	0.0306	31−33 (32%)	$P_a \rightarrow B_b(B)$
						31−32 (38%)	$P_a \rightarrow B_b(B)$
		S_4	4.77	3.01	0.0159	31−38 (24%)	
						30−34 (24%)	
		S_5	4.95	7.22	0.0003	31−36 (52%)	
						31−35 (42%)	
m-PBN[d]	(90°)	S_0		2.73			
		S_1	4.18	2.74	0.0013	28−32 (44%)	$B_a \rightarrow B_b(B)$
						29−33 (40%)	$B_b \rightarrow B_a(B)$
		S_2	4.45	2.87	0.0063	31−38 (46%)	$P_a \rightarrow P_a(A)$
						30−34 (36%)	$P_b \rightarrow P_b(A)$
		S_3	4.91	2.63	0.0187	29−32 (50%)	$B_b \rightarrow B_b(A)$
						28−33 (36%)	$B_a \rightarrow B_a(A)$
		S_4	4.93	5.56	0.0005	31−37 (70%)	
		S_5	4.94	14.79	0.0004	31−32 (52%)	$P_a \rightarrow B_b(B)$, **CT1**
						31−33 (34%)	
		S_6	5.09	2.87	0.0722	31−34 (78%)	
		S_7	5.29	16.55	0.0010	31−32 (36%)	
						31−33 (54%)	

[a] Configuration interaction (CI) analysis was performed by the inclusion of 16 frontier orbitals. [b] The orbital numbering for p-PBN at 0° differs from that given in Figure 7 because there is an orbital crossing of the HOMO1 between 0 and 23°. The assignments for 90° correspond to Figure 7. [c] Here B and P correspond to benzonitrile and pyrrole, respectively; the letters A and B in the brackets represent the symmetry within point group C_2. [d] Only approximate symmetries are given for *m*-PBN.

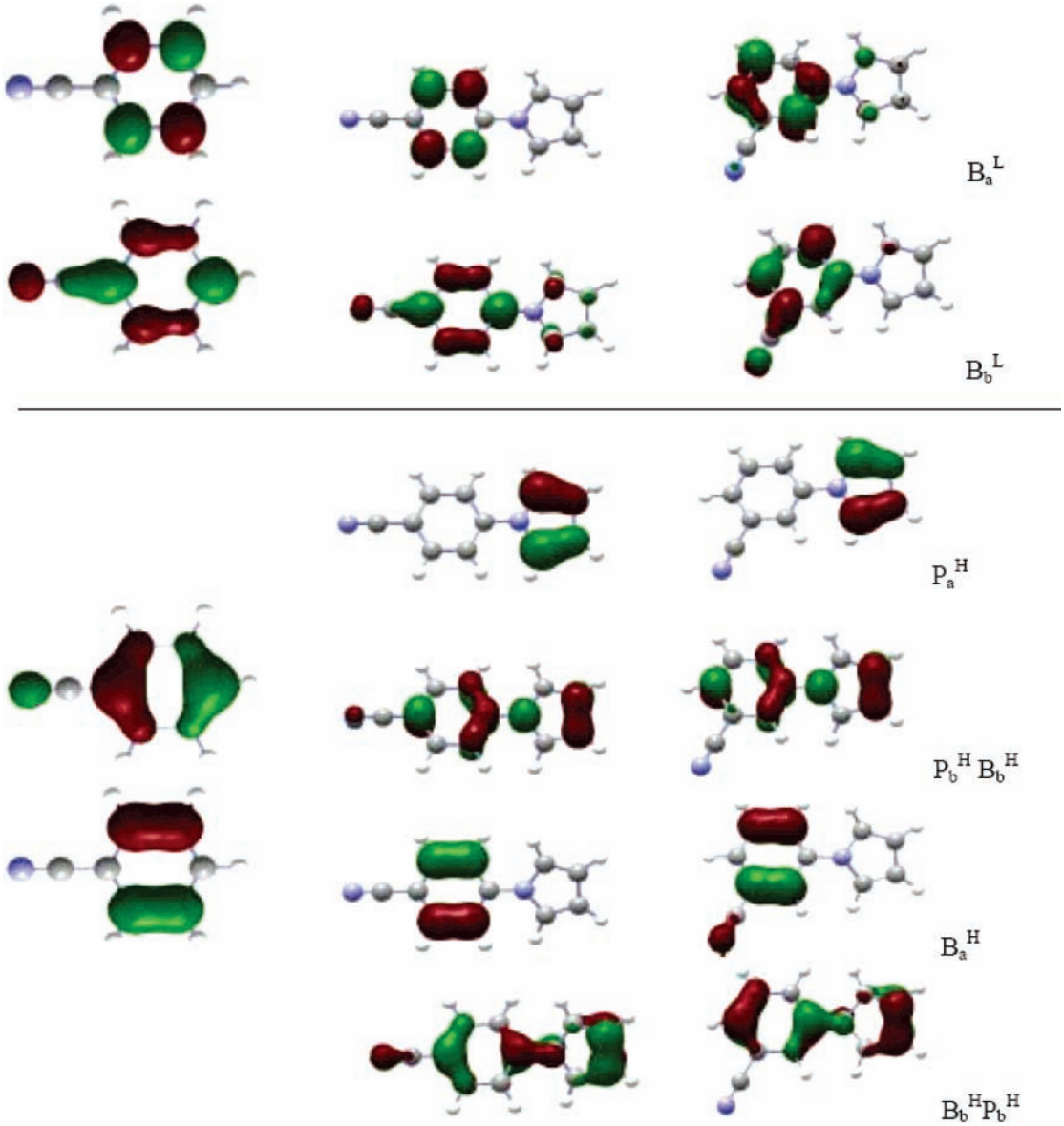

Figure 7. Highest four occupied and lowest two unoccupied molecular orbitals for *p*-PBN and *m*-PBN in the equilibrium S_0 geometry as calculated by AM1. The corresponding molecular orbitals for benzonitrile are also shown and arranged such that the coupling pattern with the orbitals of the pyrrole group becomes visible. The lower indices *a* and *b* denote subgroup orbitals transforming as symmetry species *a* and *b* in the symmetry point group C_2. As can be seen, only the subgroup orbitals of *b*-symmetry can couple leading to the a^+ (bonding) and a^- (antibonding) combination. The position of the cyano group is not important here: Even for *m*-PBN, the orbitals correspond approximately to the *a* and *b* symmetry species.

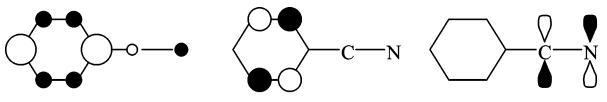

Figure 8. Lowest unoccupied MOs of benzonitrile, labeled according to C_{2v} symmetry. The corresponding symmetry species in the C_2 point group is given in square brackets (see also the lower indices of the orbitals shown in Figure 7).

the weak band is completely hidden underneath the much stronger ^1L_a-type band. Depending on the substituents, the role of ^1L_b- and ^1L_a-states as S_1 and S_2 can interchange.[24] For both *m*-PBN and *p*-PBN, the main absorption band can be assigned to the ^1L_a-state. The latter is blue shifted in the meta compound because resonance contributions are disfavored. The ^1L_b band, on the other hand, is slightly red shifted for *m*-PBN due to the meta-effect.[18] The weak shoulder around 300 nm in the absorption spectrum for *m*-PBN can therefore be attributed to the well-separated ^1L_b absorption band.

4.2. Dual Fluorescence at Room Temperature. The fluorescence maxima of *p*-PBN and *m*-PBN show a continuous red shift from nonpolar solvents to highly polar solvents indicating that a highly polar CT state is emitting in both compounds. The fluorescence spectrum of *m*-PBN in *n*-hexane appears structured and is assigned to an LE emission band ($\Delta\nu_{1/2} = 4064$ cm^{-1}). In the case of *p*-PBN, however, there is a significant broadening ($\Delta\nu_{1/2} = 6233$ cm^{-1}) of the emission spectrum, which arises due to the overlapping of two emission bands.[5] The corresponding emitting states can be assigned as LE and CT, the former one with a structured spectrum, the latter one with completely structureless emission. The low-temperature experiment (Figure 5) shows that the CT band is enhanced for *p*-PBN upon cooling. This corresponds to a situation where CT is situated energetically below LE.[5] In the more polar solvents, this energetic preference is enhanced such that no trace of structured LE emission remains visible.

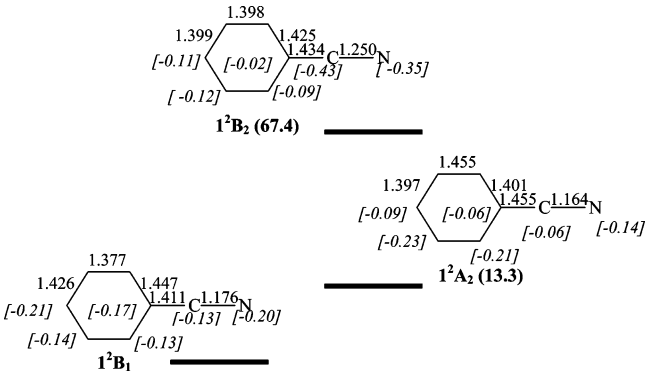

Figure 9. Optimized structure with bond lengths given, and Mulliken charges (italic numbers in square brackets of three states of the benzonitrile radical anion with different orbital occupation patterns. The 1^2B_1 state is the global minimum on the PES of the anion radical. The relative energies in kcal/mol are given in round brackets.

SCHEME 1

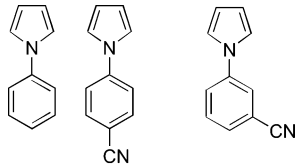

SCHEME 2: Energy Differences between the LE State (Broken Line) and the CT State (Full Line) of *p*-PBN and *m*-PBN in the Gas Phase As Calculated by AM1 and Schematic Energy Ordering of These States in Alkane Solvents

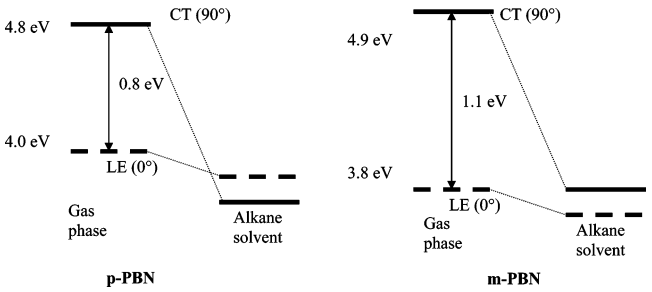

In *m*-PBN, the LE state is energetically lowered, but the CT state remains approximately at the same energy such that the energetic order is reversed in nonpolar solvents, and CT emission only appears in the more polar solvents due to the preferential lowering of the CT state. This is supported by the calculated larger energy difference in the gas phase between the LE and the higher lying CT state for *m*-PBN (1.1 eV) as compared to that of *p*-PBN (0.8 eV). The solvent *n*-hexane can therefore not stabilize the CT state of *m*-PBN below the LE state as is the case for *p*-PBN, and the appearance of a single fluorescence band for *m*-PBN is the consequence (Scheme 2). In more polar solvents, this state order is reversed.

4.3. Radiative Rates and Dipole Moments. The fluorescence rate constant k_f is significantly larger in alkane solvents as compared to polar solvents indicating a more allowed character of the emission for *m*-PBN and *p*-PBN in alkanes (Table 1). With increasing solvent polarity, there is a sudden drop of the k_f values corresponding to the change to a forbidden transition. This forbidden character present in medium and highly polar solvents for both compounds is most readily explainable by the population of a CT state with a twisted geometry (TICT state) due to the complete decoupling of the subgroup molecular orbitals.[25,26] This can also be concluded from sterically hindered model compounds like *p*-PBN with two ortho methyl groups[5] where the structured LE-features observed for *p*-PBN are absent. *p*-PBN and *m*-PBN behave similarly, with very low k_f values around 3×10^6 s^{-1} (radiative lifetimes longer than 300 ns), and comparable to the forbidden CT emission of DMABN and derivatives.[1a] The excited-state dipole moment values (Table 2) for *m*-PBN and *p*-PBN resulting from room temperature and low-temperature emission spectra are found to be similar (see ref 6). This gives additional evidence that both *m*-PBN and *p*-PBN possess the same highly polar CT state. Yoshihara et al.[6] previously determined the excited-state dipole moments for *p*-PBN and *m*-PBN, and their values are in good agreement with the values obtained in this work.

Recently, dual fluorescence has also been reported for a rigidized planar derivative of *N*-phenylpyrrole (FPP),[27] and the charge transfer nature has been compared to phenylpyrrole (PB) itself. In both cases, a red-shifted CT fluorescence band could be shown to be present in highly polar solvents. This leaves two possibilities: (i) either both FPP and PB possess a planar structure for the relaxed CT state corresponding to a "planar intramolecular charge transfer" PICT state[28−30] or (ii) FPP has a planar structure and PB a twisted one. In this case, different emissive properties are expected. Unfortunately, the experimental investigation of transition moments in PB and FPP has not been reported.[27]

These two models for the CT fluorescence in the above two compounds can be discussed in more detail in the following way:

Model A would associate the CT state with the so-called PICT state[28,31] with strong mesomeric coupling and preferred planar geometry corresponding to the ^1L_a-type state according to Platt's nomenclature. In this case, the subgroup orbitals (both symmetry species *b* in C_2) are strongly coupled and the resulting MOs are delocalized ($P_b{}^H B_b{}^H$ and $B_b{}^L$ in Figure 7), and the resulting k_f values should be large and the excited state dipole moment should be smaller than for the perpendicular and decoupled twisted CT state. The transition moment should be approximately in the long molecular axis (state with symmetry species *A* in C_2).

Model B would be associated with an electronic configuration with full orbital decoupling available also for the planar geometry. This is the case for PB and PBN,[11,26,27] if the donor orbital on pyrrole possesses a node (this is actually the HOMO in all pyrrole derivatives studied here, see the calculational results), with symmetry species *a* in C_2, and if the acceptor orbital on benzonitrile is localized, with or without a node through the carbon atom linking the benzene to the pyrrolo group ($B_a{}^L$ and $B_b{}^L$), resulting in two forbidden excited CT states of symmetry A and B, but with a very small k_f value due to this orbital decoupling even for the planar geometry.[8] According to our AM1 calculations, the lower one of these states is S_3 and is situated slightly above the PICT/^1L_a-type state (S2, see Table 4).

4.4. Theoretical Investigations. 4.4.1. AM1 Calculations. The twist angles of *m*-PBN (26.4°) and PB (26.5°) are similar in the ground state (Table 3), and both compounds have the same rotational barriers toward both planar and perpendicular geometries. In both compounds, the mesomeric interactions stabilizing the planar geometry are similarly weak. In contrast, *p*-PBN has a smaller twist angle (23.3°), leading to a smaller rotational barrier to planarity: 0.27 kcal/mol as compared to *m*-PBN (0.40 kcal/mol) and PB (0.39 kcal/mol). On the other hand, the rotational barrier (2.59 kcal/mol) of *p*-PBN toward

TABLE 5: Orbital Notations Based on C_2 Symmetry and Orbital Energies (eV) for *p*-PBN in Planar, Equilibrium, and Perpendicular Geometries

p-PBN orbital no.[a]	0°	eq	90°
33 (LUMO+1)	B_a^L (−0.15)	B_a^L (−0.17)	B_a^L (−0.25)
32 (LUMO)	B_b^L (−0.82)	B_b^L (−0.82)	B_b^L (−0.85)
31 (HOMO)	P_b^H B_b^H (−9.07)	P_a^H (−9.11)	P_a^H (−8.88)
30 (HOMO-1)	P_a^H (−9.15)	P_b^H B_b^H (−9.12)	P_b^H (−9.58)
29 (HOMO-2)	B_a^H (−10.47)	B_a^H (−10.48)	B_b^H (−10.21)
28 (HOMO-3)	P_b^H B_b^H (−10.85)	P_b^H B_b^H (−10.77)	B_a^H (−10.52)

[a] Note that there is a switching of the HOMOs between the planar and the equilibrium conformation.

perpendicularity is considerably higher than for *m*-PBN (2.05 kcal/mol) and PB (2.01 kcal/mol). These barrier changes can be directly correlated with the increased importance of the quinoid resonance structure for *p*-PBN stabilizing the planar geometry. The increased quinoid contribution can also be seen from the S_0 equilibrium structures calculated for both compounds. The benzene bond lengths are very similar for *m*-PBN, whereas in *p*-PBN, the middle benzene bonds are clearly shortened with respect to the adjacent ones.

Figure 7 and Table 4 contain AM1 results for single-point calculations of the excited state of *p*-PBN and *m*-PBN for three selected optimized ground state geometries which were performed in order to understand and assign the various excited states for differently twisted conformations. The calculations include configuration interaction between single and multiple excited configurations and are considered to contain a large part of the dynamic correlation energy. The calculated Franck−Condon energies approach quite closely the experimental absorption energies. The main absorption band (S_2) is shifted to the blue when going from *p*-PBN to *m*-PBN (due to the smaller quinoid stabilization in *m*-PBN), but the S_1 state of LE nature shifts to the red, as is typical for meta-substituted donor−acceptor benzenes.[18] In *m*-PBN, S_1 and S_2 are clearly separated (0.4 eV) and can therefore be seen as separate bands, whereas in *p*-PBN, both states are calculated to be nearly degenerate, therefore appearing as one single absorption band in the experimental spectrum.

According to AM1 calculations (Table 4) for *p*-PBN, at planarity,[32] S_1 is the forbidden ^1L_b-type state (Platt nomenclature) with *b*-symmetry in C_2 due to the overlap of same orbitals, closely followed by S_2 (*a*-symmetry, ^1L_a-type state), which possesses some CT character and is allowed due to the larger overlap. It is equivalent to the "PICT" state in the literature.[28,31] It is followed by a further state S_3 of *b*-symmetry with stronger CT (11 D) and forbidden character. This could also be called a "PICT" state but differs from the original definition[28,31] in the sense that it involves not a large but a small coupling between the molecular moieties.

The same order of states is found for the equilibrium conformation. The orbital numbering in Figure 7 corresponds to this equilibrium conformation (23°) and not to the planar one, because there is an energetic switching of the two HOMOs between these two conformations (Table 5). In both cases, S_3 corresponds to the transition involving the orbitals P_a^H and B_b^L in Figure 7.

The high dipole moment and forbidden character derives from the localized nature of P_a^H (pure HOMO of pyrrole, Figure 7), whereas the reduced dipole moment (5−6 D) and allowed character of S_2 (PICT) can be traced back to the delocalized nature of the corresponding occupied orbital ($P_a^H B_b^L$) in Figure 7.

At 90° twist, S_1 and S_2 develop into pure LE states with a small dipole moment localized on benzene and pyrrole whereas S_3 develops into the forbidden ($f = 0$) lowest TICT state of B-symmetry (CT1 with 18 D dipole moment). There are further higher lying TICT states CT2-CT3 with different symmetry, high dipole moment and $f = 0$ (see Table 4, *p*-PBN at 90°). It is important to note that the lowest TICT state of A symmetry (CT2) is situated about 0.35 eV above CT1 in this Franck−Condon geometry. As shown by the CASSCF calculations with geometry optimization,[7] this state is lowered below CT1(B) to become S_1 (see further discussion below).

4.4.2. CASSCF Calculations. When comparing the structures of the benzonitrile anion from AM1 (Figure 6) and from CASSCF ab initio (Figure 9), it is seen that AM1 only converges geometrically to the Q form, although effort was given to find the minimum of the AQ conformer also with AM1. In the neutral benzonitrile, the Q deformation is very small, but significantly larger, if benzene possesses both a donor and an acceptor substituent (*p*-PBN, Figure 6).

The CASSCF calculations show that the charge distribution in the Q and AQ conformers is quite different. In the former, much charge is localized on the atoms linking the substituent, whereas in the AQ conformer, most negative charge is concentrated on the four central carbon atoms. The Q conformer (1^2B_1) is more stable than the AQ (1^2A_2) one. In terms of orbital involvement, the Q (1^2B_1) state possesses a singly occupied orbital with an antinode through the linking atoms (B_b^L in Figure 7), the AQ (1^2A_2) state a singly occupied orbital with a node through the linking atoms (B_a^L in Figure 7).

When the AQ radical anion conformer of benzonitrile is linked to a π-system at any twist angle such that a CT state is formed, (e.g., linkage to the pyrrolo radical cation in *p*-PBN), the overall symmetry point group is reduced to C_2, and Q and AQ states of benzonitrile radical anion are of A and B symmetry, respectively, and the singly occupied orbitals similarly. The CT transition from pyrrole to benzonitrile can involve orbitals of the same or of different symmetry on the pyrrolo unit. In the Q state of A symmetry (as calculated in ref 7), the singly occupied orbital on pyrrole must have an antinode through the linking atom (P_b^H in Figure 7) in order to yield an overall symmetry species A. In the AQ state of A symmetry, both singly occupied orbitals on the two units must have B symmetry in order to yield the overall symmetry A. This means that the planar Q-CT state of A symmetry in PBN involves the transition between orbitals $P_b^H B_b^H$ and B_b^L in Figure 7 with strong coupling through orbital delocalization, but the AQ-CT state of A symmetry involves the orbitals P_a^H and B_a^L with a node between pyrrole and benzonitrile moieties giving the possibility for free rotation of sub moieties. This can be nicely followed by the CASSCF calculation, which shows that for intermediate twist angles, these two conformation mix through configuration interaction. The single occupancy of B_a^L in the AQ state explains both the long central bonds in benzene (orbital node between the central atoms) and the accumulation of negative charge on the adjacent atoms (orbital coefficients only on these atoms in B_a^L).

There are, of course, further CT states present which can most readily be identified at 90° twist. There is a further A state with CT between P_b^H and B_b^L which corresponds in nature to the TICT state in DMABN. And there are two further CT states of B symmetry, combining the orbital pairs P_b^H with B_a^L and P_a^H with B_b^L (see Figure 7). All these states have been calculated for the rigid ground-state geometry with AM1 and are contained in Table 4 (last column).

The main discrepancy between the CASSCF optimized

excited-state energies (ref 7) and the semiempirical (this work) or DFT/MRC results for the rigid geometries[33] is that the A-CT of AQ character is the lowest CT state at 90° after geometrical relaxation[7] whereas for the Franck−Condon situation, the CT state of B symmetry (and Q character involving B_b^L and P_a^H) is the lowest one. We conclude that the excited-state geometrical relaxation must switch these two CT states.

We can also conclude on the two CT states present in DMABN for 90° twist: Because the amino group possesses a donor orbital of B symmetry, two of the CT states in PBN (involving P_a^H) must be absent in DMABN. The lowest TICT state is of A symmetry involving the B_b^L orbital on benzonitrile. We therefore expect that this TICT state has the Q bond length pattern in benzonitrile, as found by all calculations until now. But the second TICT state, somewhat higher lying in energy, will be of B symmetry and involve B_a^L as accepting orbital and is therefore expected to possess the AQ bond length pattern.

Finally, due to the localized LUMO for *m*-PBN (Figure 7), we can likewise expect that the geometry-relaxed lowest CT state at 90° will be an AQ state of A symmetry, similarly as in *p*-PBN.

5. Conclusions

The comparison of the meta- and para-derivatives of 4-cyanophenylpyrrole (PBN) shows that, in both cases, forbidden emission from a highly dipolar state is observed. The forbiddenness is associated with a twist to angles close to perpendicularity (TICT state). This occurs similarly for the meta derivative, which is the first case where a meta compound is shown to be able to populate a TICT state. Quantum chemical CI calculations of semiempirical (AM1) and ab inito (CASSCF) quality are compared and the different states are characterized by their orbital transitions. meta-PBN shows roughly similar orbitals to *p*-PBN which explains the very similar excited-state behavior.

The main results from the calculations are as follows: (a) that the quinoid to antiquinoid transition in the excited state of PBN is already present in the benzonitrile radical anion (which is part of the PBN CT state) and there can occur likewise for the para and the meta derivative and (b) that there is a state switching between the lowest TICT states of A and B symmetry by geometrical relaxation in the excited state.

Acknowledgment. We kindly acknowledge Shmuel Zilberg, Department of Physical Chemistry and the Farkas Center for Light Induced Processes, The Hebrew University of Jerusalem, Jerusalem, Israel, for performing the CASSCF calculations. We thank A. Ratzinger for the synthesis of *m*-PBN.

References and Notes

(1) (a) Rettig, W. *Angew. Chem., Int. Ed. Engl.* **1986**, *25*, 971. (b) Grabowski, Z. R.; Rotkiewicz, K.; Rettig, W. *Chem. Rev.* **2003**, *103*, 3899.

(2) Lippert, E.; Lüder, W.; Boos, H. *Adv. Mol. Spectrosc. Proc. Int. Meet. 4th 1959* 1962, 443.

(3) Rettig, W.; Bliss, B.; Dirnberger, K. *Chem. Phys. Lett.* **1999**, *305*, 8.

(4) Zachariasse, K. A.; von der Haar, T.; Hebecker, A.; Leinhos, U.; Kuehnle, W. *Pure App. Chem.* **1993**, *65*, 1745.

(5) Cornelissen-Gude, C.; Rettig, W. *J. Phys. Chem. A* **1998**, *102*, 7754.

(6) Yoshihara, T.; Galievsky, V. A.; Druzhinin, S. I.; Saha, S.; Zachariasse, K. A. *Photochem. Photobiol. Sci.* **2003**, *2*, 342.

(7) Zilberg, S.; Haas, Y. *J. Phys. Chem. A* **2002**, *106*, 1.

(8) Rettig, W.; Marschner, F. *Nouv. J. Chim.* **1983**, *7*, 425.

(9) Pinto, D. J. P.; Orwat, M. J.; Wang, S.; Fevig, J. M.; Quan, M. L.; Amparo, E.; Cacciola, J.; Rossi, K. A.; Alexander, R. S.; Smallwood, A. M.; Luettgen, J. M.; Liang, L.; Aungst, B. J.; Wright, M. R.; Knabb, R. M.; Wong, P. C.; Wexler, R. R.; Lam, P. Y. S. *J. Med. Chem.* **2001**, *44* (4), 566.

(10) Parker, C. A. *Photoluminescence of Solutions*; Elsevier: Amsterdam, 1968.

(11) (a) Meech, S. R.; Phillips, D. *J. Photochem.* **1983**, *23*, 193. (b) Velapoldi, R. A.; Epstein, M. S. *ACS Symp. Ser.* **1989**, *383*, 98.

(12) O'Connor, D. V.; Phillips, D. *Time Correlated Single Photon Counting*; Academic Press: London, 1984.

(13) Globals Unlimited, Laboratory of Fluorescence Dynamics at the University of Illinois, 1992.

(14) Dewar, M. J. S.; Zoeblich, E. G.; Healy, E. F.; Stewart, J. J. P. *J. Am. Chem. Soc.* **1985**, *107*, 3202.

(15) AMPAC 6.0 and AMPAC 6.55, Semichem, Inc., Shawnee Mission, KS, 1997.

(16) Schmidt, M. W.; Baldrige, K. K.; Boatz, J. A.; Elbert, S. T.; Gordon, M. S.; Jensen, J. H.; Koseki, S.; Matsunaga, N.; Nguyen, K. A.; Su, S J.; Windus, T. L.; Dupuis, M.; Montgomery, J. A. *J. Comput. Chem.* **1993**, *14*, 1347.

(17) Dunning, T. H., Jr. *J. Chem. Phys.* **1989**, *90*, 1007; basis sets were obtained from the Extensible Computational Chemistry Environment Basis Set Database, Version 02/25/04, as developed and distributed by the Molecular Science Computing Facility, Environmental and Molecular Sciences Laboratory which is part of the Pacific Northwest Laboratory, P.O. Box 999, Richland, WA 99352, and funded by the, U.S. Department of Energy.

(18) Grinter, R.; Heilbronner, E.; Godfrey, M.; Murrell, J. N. *Tetrahedron Lett.* **1961**, *21*, 771.

(19) Maus, M.; Rettig, W.; Bonafoux, D.; Lapouyade, R. *J. Phys. Chem. A* **1999**, *103*, 2288.

(20) Lippert, E. *Z. Naturforsch.* **1955**, *10a*, 541. Mataga, N.; Kaifu, Y.; Kazumi, M. *Bull. Chem. Soc. Jpn.* **1955**, *28*, 690; **1956**, *29*, 465.

(21) Riddick, J. A.; Bunger, W. B.; Sakano, T. K. *Organic Solvents*; John Wiley & Sons: 1986.

(22) Rösch, N.; Zerner, M. C. *J. Phys. Chem.* **1994**, *98*, 5817.

(23) Belau, L.; Haas, Y.; Rettig, W. *Chem. Phys. Lett.* **2002**, *364*, 157.

(24) Rettig, W.; Wermuth, G.; Lippert, E. *Ber. Bunsen-Ges. Phys. Chem.* **1979**, *83*, 692. Wermuth, G. *Z. Naturforsch.* **1983**, *38a*, 368. Wermuth, G.; Rettig, W. *J. Phys. Chem.* **1984**, *88*, 2729.

(25) Rettig, W.; Marschner, F. *New. J. Chem.* **1990**, *14*, 819.

(26) Rettig, W. *J. Mol. Struct.* **1982**, *84*, 303.

(27) Yoshihara, T.; Druzhinin, S. I.; Zachariasse, K. A. *J. Am. Chem. Soc.* **2004**, *126*, 8535.

(28) Zachariasse, K. A. *Chem. Phys. Lett.* **2000**, *320*, 8.

(29) Il'ichev, Yu. V.; Kühnle, W.; Zachariasse, K. A. *J. Phys. Chem. A* **1998**, *102*, 5670.

(30) Zachariasse, K. A.; Grobys, M.; von der Haar, Th.; Hebecker, A.; Il'ichev, Yu. V.; Jiang, Y.-B.; Morawski, O.; Kühnle, W. *J. Photochem. Photobiol., A* **1996**, *102*, 59. Erratum: *J. Photochem. Photobiol., A* **1998**, *115*, 259.

(31) von der Haar, T.; Hebecker, A.; Ii'ichev, Y.; Jiang, Y.-B.; Kuehnle, W.; Zachariasse, K. A. *Pays-Bas* **1995**, *114*, 430.

(32) It is assumed here, that the increased mesomeric interaction in the excited states leads to a planar minimum for the lowest excited states. This is supported by the very low barrier to planarity in the ground state.

(33) Parusel, A. B. J. *Phys. Chem. Chem. Phys.* **2000**, *2*, 5545.